Langmuir

Article

pubs.acs.org/Langmuir

Effect of Ionization on the Behavior of *n*-Eicosanephosphonic Acid Monolayers at the Air/Water Interface. Experimental Determinations and Molecular Dynamics Simulations

Erica P. Schulz,*[,†] Ángel Piñeiro,[‡] José Miñones, Jr.,[§] José Miñones Trillo,[§] Marisa A. Frechero,[†] Olga Pieroni,[†] and Pablo C. Schulz[†]

[†]Departamento de Química e INQUISUR, Universidad Nacional del Sur y CONICET, Bahía Blanca, Argentina

[‡]Soft Matter & Molecular Biophysics Group, Department of Applied Physics and [§]Departamento de Química Física, Facultad de Farmacia, University of Santiago de Compostela, CP 15872, Santiago de Compostela, Spain

Supporting Information

ABSTRACT: Monolayers of *n*-eicosanephosphonic acid, EPA, were studied using a Langmuir balance and a Brewster angle microscope at different subphase pH values to change the charge of the polar headgroups (Z_{av}) from 0 to −2. Molecular dynamics simulations (MDS) results for $|Z_{av}| = 0$, 1, and 2 were compared with the experimental ones. EPA monolayers behave as mixtures of mutually miscible species ($C_{20}H_{41}-PO_3H_2$, $C_{20}H_{41}-PO_3H^-$, and $C_{20}H_{41}-PO_3^{2-}$, depending on the subphase pH). The order and compactness of the monolayers decrease when increasing $|Z_{av}|$, while go from strongly interconnected by phosphonic−phosphonic hydrogen bonds ($|Z_{av}| = 0-0.03$) through an equilibrium between the total cohesive energy and the electrostatic repulsion between the charged polar groups ($0.03 < |Z_{av}| < 1.6$) to an entirely ionic monolayer ($|Z_{av}| \approx 2$). MDS reveal for $|Z_{av}| = 0$ that the chains form spiralled nearly rounded structures induced by the hydrogen-bonded network. When $|Z_{av}| \approx 1$ fingering domains were identified. When $Z \approx 2$, the headgroups are more disordered and distanced, not only in the *xy* plane but also in the *z* direction, forming a rough layer and responding to compression with a large plateau in the isotherm. The monolayers collapse behavior is consistent with the structures and domains founds in the different ionization states and their consequent in-plane rigidity: there is a transition from a solid-like response at low pH subphases to a fluid-like response at high pH subphases. The film area in the close-packed state increases relatively slow when the polar headgroups are able to form hydrogen bonds but increases to near twice that this value when $|Z_{av}| \approx 2$. Other nanoscopic properties of monolayers were also determined by MDS. The computational results confirm the experimental findings and offer a nanoscopic perspective on the structure and interactions in the phosphonate monolayers.

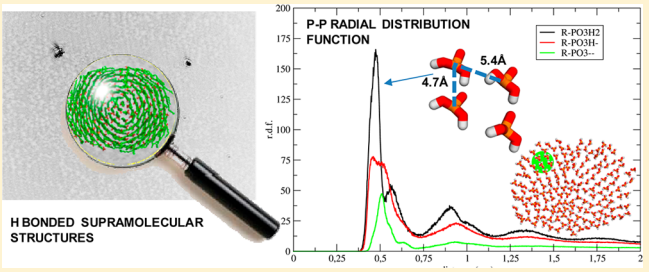

INTRODUCTION

Interfaces are ubiquitous in nature, and by mimicking nature it is possible to take advantage of interface-based systems. In order to rationally control membrane properties of a certain system, it is convenient to previously get knowledge of monolayers and films built with the same molecules. The solution pH affects many membrane-mediated biological processes. However, the mechanisms utilized by membranes of cells and cellular organelles to maintain integrity is still not well understood, constituting an important biophysical problem. Zhou and Raphael[1] characterized the effect of pH on the electrical and mechanical properties of 1-stearoyl-2-oleoylphosphatidylcholine, concluding that these properties are interconnected, supporting the emerging paradigm of the membrane as an electromechanical structure.

Alkanephosphonic acids charge (Z) can be tuned as 0 ($R-PO_3H_2$), −1 ($R-PO_3H^-$), or −2 ($R-PO_3^{2-}$) by changing the medium pH. They are weak acids with some interesting properties. In the micelles, the Stern layer is connected by hydrogen bonds from charge near 0 up to an average charge of −1.[2,3] The phase behavior depends on the charge. Alkanephosphonic acids give rise to lamellar liquid crystals when solid is in contact with water.[2,4] Mono- and disodium alkanephosphonates produce hexagonal mesophases.

A study on soluble monolayers of alkanephosphonic acids at the air/water interface[2] demonstrated their strongly nonideal behavior and compactness, which is not the common case for soluble surfactants, suggesting a tight union of the polar headgroups by hydrogen bonding. These hydrogen bonds also appear in the polar layer at the hydrocarbon/water interface in alkanephosphonic acid-stabilized emulsions.[5] The hydrogen-bonded structure at the emulsion droplets interface shows significant changes from a strongly bonded to a less compact layer formed by $-PO_3H_2$ and $-PO_3H^-$ groups favoring

Received: June 25, 2014
Revised: February 6, 2015

ACS Publications © XXXX American Chemical Society

DOI: 10.1021/la5050283
Langmuir XXXX, XXX, XXX−XXX

inversion from O/W to W/O/W emulsion when the surfactant has a neutralization degree of about 0.47, i.e., is composed by about a equimolecular mixture of $R-PO_3H_2$ and $R-PO_3H^-$ species.[6] Klose et al.[4] found the formation of hydrogen bonds in the polar layer of lamellar liquid crystals of *n*-alkanephosphonic acids of low molecular weight. Micelles of *n*-dodecanephosphonic acid do also have their polar headgroups connected by hydrogen bridges, maintaining their structure upon neutralization when the average charge (in absolute value) is $Z_{av} = 1$.[2]

Molecular dynamics simulations offer a nanoscopic perspective that combined with experimental analysis provide a multilevel characterization of nanoaggregates and monolayers.[7,8] Many investigations using molecular dynamics simulations of nanoaggregates spontaneously formed in the bulk solution[9] or at the air/water interface[10] have been reported not only for their scientific interest but also for the industrial, pharmaceutical, and medical[11] applications. Duncan and Larson[12] thoroughly compared simulated, obtained both by coarse-grained and by atomistic models, and experimental pressure−area isotherms for dipalmitoylphosphatidylcholine (DPPC) monolayers and explore possible factors influencing the shape and position of the isotherms and the discrepancies between simulated and experimental isotherms.

A wide spectrum of dynamical events occur at different time and length scales in monolayers, from ordering and phase transitions in two dimensions through surface undulations and capillary waves to collapse transitions in three dimensions. Several parameters available from molecular dynamics simulations results, such as order parameters, extension of the chains, thickness of the monolayer, tilting of surfactant chains, the relative azimuth between molecules or domains, and their depth into the subphase, have been defined in order to characterize in an atomistic resolution Langmuir monolayers, where surfactant molecules are constrained to lie in a plane.

The surface properties of alkanephosphonic acids, apart from the pure physical chemistry interest, will help to elucidate the role of the phosphonate group in many applications, such as their plausible use in protocells.[13] Phosphonates are in general biocompatible and innocuous. They have been used to increase the chemical interaction between titanium implants and bones.[14]

Phosphonic acids are especially promising for surface modifications of a wide variety of solid surfaces,[15] such as gold, titanium, mica, and various oxides (TiO_2, ZrO_2, Al_2O_3, and $BaTiO_3$), due to the their ability to form robust monolayers without the need to resort to cross-linking and the significance of the systems composed of these molecules (electrical and biological sensor applications and corrosion inhibitors). They also have applications in different branches of industry such as flotation,[16] corrosion inhibition,[17] and emulsion formulation,[6] among others. Because of their capacity for retaining water, their thermal stability, and their capacity to form hydrogen-bonded networks, phosphonic acids have been proposed for the development of membranes for proton exchange in fuel cells.[18] Since phosphonic acids were found in meteorites such as the Murchison one,[19] and it is possible to synthesize them in the conditions of prebiotic Earth,[20,21] it has been proposed that cellular protomembranes may be composed of phosphonates, possibly mixed with fatty acids.

Among the new applications of self-assembled surfactant monolayers, we can mention their use as drug delivery agents,[22] chemical microreactors for nanofabrications purposes,[23] molecular coatings with specific properties, microelectronic, templates for nanolithography,[24] and nanoelectromechanical and microfluidic devices and compounds for organic solar cells.[25]

To the best of our knowledge, there are no studies on the surface behavior of insoluble monolayers of alkanephosphonic acids and their salts at the air/water interface. However, some old studies on the related alkylphosphoric acids[26] together with the results on soluble monolayers led us to focus our work on the insoluble monolayers of alkanephosphonic acids. In view of the multiple applications in many technology and research fields, especially in the elucidation of the origins of life (*vide supra*), we believe that a thorough knowledge of the behavior and the control variables of phosphonate monolayers is essential to move forward into cutting-edge technology and new research theories.

We have studied the monolayers of *n*-eicosanephosphonic acid ($C_{20}H_{41}PO_3H_2$) spread on aqueous subphase having different pH values in order to analyze the effect of changing the average charge of the polar headgroup from 0 to −2. This study has been performed both experimentally, with a Langmuir balance and a Brewster angle microscope, and theoretically, by means of molecular dynamics simulations (MDS). Results from both techniques were in strong agreement.

EXPERIMENTAL SECTION

Experimental Measurements. The eicosanephosphonic acid (EPA) was synthesized according to the Kosolapoff procedure.[27] It was dissolved in an ethanol:chloroform mixture 1:4 (v/v) with two drops of pentanol to favor spreading. The EPA solution with a concentration of 0.330 mg mL^{-1} was kept in a fridge at ∼5 °C in a sealed vial between measurements.

The subphases were made with ultrapure water, obtained from a Milli-RO, Milli-Q reverse osmosis system (Millipore) (18 MΩ cm^{-1} resistivity, pH = 6). Teorell and Stenhagen buffers[28] were prepared with different pH values: 1.8, 3.7, 6.3, 8.0, 9.9, and 11.8, having an ionic strength of about 0.4. These values were chosen in order to cover the entire range of ionization states of the EPA determined using the pK_{a1} and pK_{a2} of the acid, which were not measured because of the very low water solubility of the acid. We used the computed values $pK_{a1} = 5.48$ and $pK_{a2} = 9.92$ (see the Supporting Information for the details of the calculation of the ionization states). The absolute values of the average charge per headgroup (Z_{av}) corresponding to the pH values used in the present work have been determined using Figure 1 in the Supporting Information and are shown in Table 1. It is worth noting that the formation of hydrogen bridges between adjacent phosphonic acid groups was postulated by Gershfeld and Pak[26] as the reason for the increase in the surface pK_a values of *n*-alkylphosphoric acids monolayers from that observed in bulk solutions as well as for the increase of the surface viscosity with time due to the formation of aggregates.

Table 1. Absolute Average Values of the Charge of the Adsorbed Molecules (Z_{av})

subphase pH	1.79	3.70	6.35	8.01	9.90	11.81
Z_{av}	0.00	0.03	0.73	0.997	1.99	2.00

The monolayers were studied in a Langmuir film balance Nima 601 BAM with a balance trough maximum surface of 500 cm^2 and a minimum area of 41 cm^2. The compression speed was 10 cm^2 min^{-1} or 1.8 $Å^2$ $molecule^{-1}$ min^{-1}. All measurements were made at room temperature: 23.0 ± 0.5 °C. In order to ensure the complete evaporation of the solvent, we waited 15 min before starting the

DOI: 10.1021/la5050283
Langmuir XXXX, XXX, XXX−XXX

compression. The surface pressure (Π) was measured to an accuracy of 0.1 mN m^{-1}.

Brewster angle microscopy (BAM) images obtained during the compression process were recorded using a NFT BAM 2000 ellipsometer (Göttingen, Germany) placed on the Nima film balance whose trough is large enough to mount the microscope directly on it. The BAM is equipped with a 30 mW laser emitting p-polarized light with a wavelength of 532 nm which was reflected off at the air/water interface at the Brewster angle (53.1°). Under such condition, the reflectivity of the beam was almost zero on the pure water interface. The reflected beam passed through a focal lens, into an analyzer at a known angle of incident polarization, and finally to a CCD camera. The lateral resolution of the microscope was 2 μm, and the shutter speed used was 1/50 s. The images were digitalized and processed to optimize image quality (see Supporting Information); those shown below correspond to 768 × 572 pixels.

The equilibrium spreading pressures Π_e for the different systems were determined by measuring the surface tensions with a semi-automatic Krüss EasyDyne tensiometer using the platinum Wilhelmy plate. This pressure is spontaneously generated when EPA crystals are put in contact with the liquid surface. At any surface pressure higher than Π_e there is a tendency of the molecules to aggregate in crystals. However, the process is so slow that the monolayers are in metastable equilibrium and may be worked without collapse.[29] Powdered crystals of EPA were spread on the different subphases and left for 4 days to allow the attainment of equilibrium before measuring the surface tension. The surface tensions of the clean subphases were also measured. To avoid atmospheric contamination, the samples were maintained in the measuring vessels sheltered by plastic covers. Figure 4 in the Supporting Information shows the plot of the equilibrium spreading pressure Π_e as a function of the subphase pH (or Z_{av}). Π_e is 11.7 mN m^{-1} between pH 4 and 8; then it suddenly raises up to 25 at pH = 9 and gradually descends to 4.9 at pH = 13.

Molecular Dynamics Simulations. *Setup of the Simulation Boxes.* MD simulation studies of the *n*-eicosanephosphonic acid and its mono and two-charged salts were performed to investigate the formation of self-assembled monolayers. Each system was built by placing the surfactant molecules at random positions and orientations in a 7 × 6 × 6 nm box which was then filled with water molecules and the necessary amount of counterions in order to electrically neutralize the charged surfactants. An energy minimization using the steepest descent method was carried out. The *z* dimension of the simulation box was then extended to 24 nm to allow the formation of two air/water interfaces perpendicular to this axis. Then a 10 ns long MD simulation at 298 K and constant volume produced two monolayers of surfactant molecules at the surface of the solution. Afterward, the system was enlarged by a factor of 4 pasting two inverted copies of itself adjacent to the original box in the *xy* plane and an exact replica in the diagonal, as described in a previous work.[10] The resulting systems consisted in 340 $C_{20}H_{41}-PO_3H_2$ molecules and 18 724 water molecules; 340 $C_{20}H_{41}-PO_3H^-$ and 340 H_3O^+ plus 15 944 H_2O molecules; and 480 $C_{20}H_{41}-PO_3^{2-}$ plus 960 H_3O^+ with 13 184 H_2O molecules, respectively. Taking these boxes as initial configuration, three sets of 30 ns constant volume MD simulations at 298 K were performed.

MD Simulation Parameters. All simulations were performed using the GROMACS package,[30] version 4.5.1. The surfactant molecules were modeled using the GROMOS96(53a6)[31] force field with the bonded parameters and partial charges adapted from Roy et al.[18] The simple point charge (SPC) model[32] was utilized for water molecules. Periodic boundary conditions with rectangular boxes were used. Water and surfactant molecules were separately coupled to a V-rescale thermostat with a common period of 0.1 ps. Long-range electrostatic interactions were calculated using the particle mesh Ewald method with a real-space cutoff of 1.2 nm, a 0.15 spaced grid, and a fourth-order B-spline interpolation. The Ewald sum in three dimensions with a correction term (EW3DC) was used to avoid artifacts due to interactions between replicas in the *z* direction. No dispersion correction was considered for the short-range van der Waals interactions which were evaluated with a cutoff of 2.8 nm to approach better the surface tension of the solutions. Random initial velocities were assigned to the systems from a Maxwell–Boltzmann distribution at 298 K. The equations of motion were integrated using the leapfrog method with a time step of 2 fs. Bond lengths and angles in water were constrained using SETTLE algorithm[33] while the LINCS[34] algorithm was used to constrain bond lengths within the surfactant molecules.

RESULTS AND DISCUSSION

For the sake of clarity and ease of comparison, the isotherms obtained in the pH range studied are all grouped in Figure 1. Three different behaviors may be identified and are indicated with different colors.

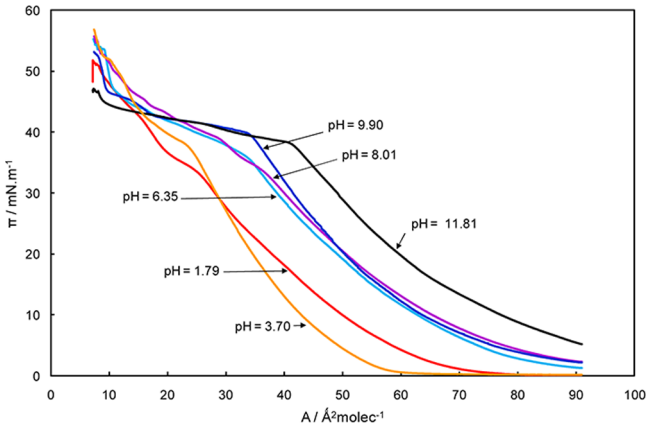

Figure 1. Comparison of representative isotherms as a function of the subphase pH. Red and orange: $Z_{av} < 0.03$; light blue, purple, and blue: $0.03 < Z_{av} < 1.6$; black: $Z_{av} = 2$.

Monolayers Behavior at Subphase pH Values of 1.8 and 3.7. Representative Π (surface pressure)–*A* (area per molecule) isotherms of EPA monolayers spread on subphases with pH 1.8 ($Z_{av} = 0$) and pH 3.7 ($Z_{av} = 0.03$) are shown in Figure 5 of the Supporting Information. The contraction observed in the Π–*A* isotherms when the subphase pH is raised from 1.8 to 3.7 (Figure 1), where the little film dissociation would be expected to expand the monolayer, has been also observed by Gershfeld and Pak[26] in monooctadecyl phosphate monolayers when the pH was raised from 4.9 to 5.8 and was interpreted on the basis that the total cohesive energy of the monolayer, which includes the van der Waals interactions among the hydrocarbon chains, the hydration effects, and the interactions among the neighboring headgroups, exceeds the increase of the repulsion when the acids headgroups are ionized. This effect is more pronounced at surface pressures below 30 mN m^{-1}, when the headgroups are far apart and the repulsion between them is very small.

Both isotherms show discontinuities which usually denote the existence of phase transitions along the compression of the monolayer. According to the compressional modulus value limits (see insets in the isotherms in the Supporting Information), the monolayers would be in the liquid-expanded state since $\kappa^{-1} < 50$ mN m^{-1} (inset of Figure 5 in the Supporting Information). This situation is repeated in the other isotherms. However, the tendency of the EPA molecules to form phosphonic–phosphonic hydrogen bonds on acidic subphases causes the formation of numerous small islands of condensed phase separated from each other by a gas phase, as observed by BAM (Figure 2a) and confirmed by the MDS (see below). The visualization by BAM of floating islands of

DOI: 10.1021/la5050283
Langmuir XXXX, XXX, XXX–XXX

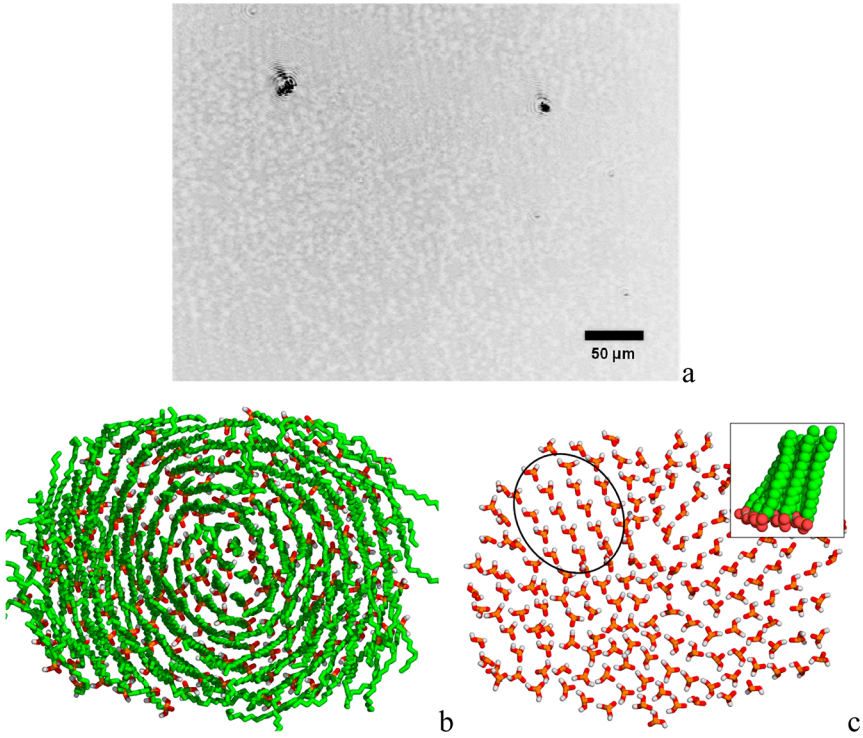

Figure 2. (a) BAM image of the monolayer at pH 1.79, Π = 2.1 mN m^{-1}, and A = 90 $Å^2$ $molecule^{-1}$, showing a dispersion of small islands of condensed phase in a gaseous matrix. (b) Upper view of the simulated spiraled island of $C_{20}H_{41}-PO_3H_2$ monolayer (hydrocarbon chains in green; P in orange; O in red; and H in white). (c) Headgroups disposition with a regular arrangement highlighted. Inset: molecules disposition in the regular arrangement.

condensed phase in a gas phase of long chain fatty acids on an acidified subphase at high molecular areas and very low surface pressures has been reported in the literature.[35] Besides, the point at which the surface pressure first rises has been ascribed to that at which these domains contact each other.

The formation of islands with compact and rounded morphology of octadecylphosphonic acid molecules adsorbed on mica surfaces[36] has been attributed to a rearrangement of the adsorbed molecules and to the existence of a significant effective line tension between the islands and the "bare" areas, which in turn are interpreted as completely free of surfactant molecules or formed by an extremely thin and delicate layer of adsorbed molecules. In this paper the islands were interpreted as being in solid state. The isotherm of octadecylphosphonic acid on water at 22 °C presents two kinks: at 21 and at 18.8 $Å^2$/molecule. Another work also documents the nucleation of submonolayer islands in the formation process of a self-assembled monolayer of octadecylphosphonic acid deposited from solution.[37]

A visual inspection of the simulated $C_{20}H_{41}-PO_3H_2$ monolayers reveals the formation of rounded and spiraled islands as shown in Figure 2b. The headgroup disposition in this monolayer is shown in Figure 2c, where a cluster of regularly arranged headgroups is highlighted. The conformation adopted by the molecules in those clusters is shown in the inset. The close packing of insoluble monolayers often causes the formation of structures with long-range two-dimensional order.[38] The condensed phase in which the molecules are tilted away from the vertical at a consistent angle and toward their nearest neighbors is denominated L_2 phase,[35] a two-dimensional liquid-crystalline phase with bond orientational order in the position of the headgroups that is analogous to the smectic-I phases of liquid crystals. For fatty acids the phase sequence along compression[34] is G → G + LE → LE → LE + L_2 → L_2 → LS (vertical condensed phase) → S. As explained by Rosoff,[35] the initial portion of the isotherm of stearic acid on an acidified subphase has often been erroneously assigned as the disordered liquid phase, whereas it is actually the L_2 phase. Analogously, the low compressional modulus values suggesting a LE behavior of the EPA monolayer can be misinterpreted on the basis of the individual molecules interaction while the interacting units on compression are the islands.

A careful examination of the headgroup atoms disposition in the simulated monolayers (Figure 2c) allows the detection of radial strings and clusters of regularly arranged atoms that seem to be responsible for the formation of the spirals. The molecules in these clusters adopt a sort of twisted parallelepiped shape (inset Figure 2c), and the molecules in the strings are also tilted. The double bonded O and the hydroxyl groups of each phosphonic group form in the surface plane a scalene triangle whose sides, computed using literature data,[39] are 0.239 nm between the OH groups and 0.251 and 0.255 nm between each of the −OH and the double bonded O. These dimensions are shown for one of the simulated molecules in the inset of Figure 6 in the Supporting Information. This triangle is the base of a pyramid (i.e., the headgroup) where the edges are 0.147 nm for the P═O and 0.154 nm for the P−OH. The angles between each of the P−OH and the P═O bonds are 113° and 116°, respectively, while the angle between both the P−OH bonds is 102°. Figure 6 in the Supporting Information shows the disposition of the regularly arranged headgroups with the distances between phosphorus atoms. The distance between oxygens in a hydrogen bond is 2.62 Å. In Figure 7 in the Supporting

DOI: 10.1021/la5050283
Langmuir XXXX, XXX, XXX−XXX

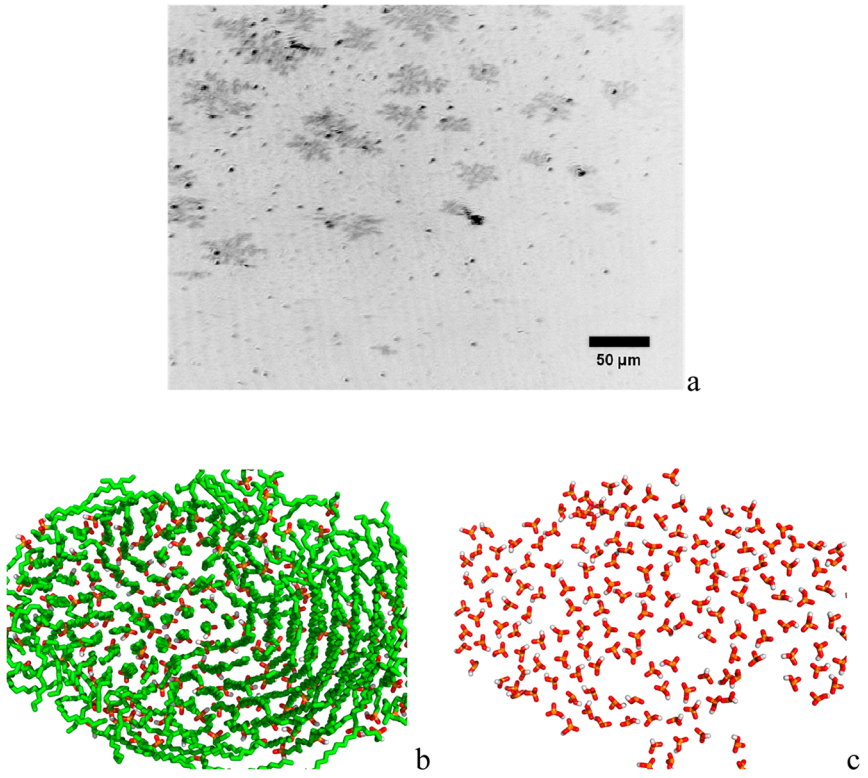

Figure 3. (a) BAM image of the EPA monolayer spread on subphase of pH = 6.35 (Z_{av} = 0.73) in the first break in the Π–*A* isotherm (Π = 40 mN m^{-1} and *A* = 25 $Å^2$ $molecule^{-1}$) showing fingering domains. (b) Upper view of the simulated $C_{20}H_{41}$–PO_3H^- monolayer (hydrocarbon chains in green; P in orange; O in red; and H in white). (c) Headgroups disposition. Notice the formation of lobules.

Information it can be appreciated, in a lateral view of the $C_{20}H_{41}$–PO_3H_2 monolayer, that there are zones where the hydrocarbon chains are more erected. According to reflection–absorption FT-IR measurements,[40] numerous *gauche* bonds in the chains correspond to expanded phases while highly ordered chains with mostly *trans* bonds are present in condensed phases.

Then, the present simulation results agree with the above experimental findings of small islands floating on an almost free water surface in monolayers with $Z \approx 0$ (Figure 2a). The simulated islands are formed by all the available molecules and increasing the system dimension would probably lead to bigger islands. From the BAM image above it can be appreciated that the islands have micrometer-order size and that the amount of surfactant is not enough to cover the entire surface as happens in the simulations. An island of 4 μm of radius has a 50 μm^2 area approximately (5×10^7 nm^2), and thus it is composed of about 10^9 molecules. Therefore, it is impossible to simulate a complete island, but the experimentally observed islands may be considered as an extrapolation of the simulated islands.

In a literature work[36] round octadecanephosphonic acid islands adsorbed on mica increase in size and grow together with time, and finally only small holes remained in the film which gradually are filled. This could be considered to be equivalent to a compression of the EPA monolayer: the islands are pushed together and eventually fill the entire surface when the collapse starts. Hydrogen bonds are probably formed among islands in contact, giving a network extended to the entire monolayer.

Collapse is broadly defined as the movement of surfactant molecules from the interface into the bulk, i.e., a two-to-three-dimensional phase transition under overcompression. Modified structures are formed in the direction perpendicular to the water surface. Thus, the compressive stresses eventually relax adopting some nonflat or out-of-plane geometry by either a fluid-like response through a nucleation and growth mechanism or a solid-like response involving large undulations (folding) of the surfactant layer which has been found to depend on the in-plane rigidity.[41,42] There are two main collapse behaviors: either π falls suddenly after a collapse pressure π_c (denominated "constant area collapse" and observed for fatty acid monolayers on pure water) or it remains nearly constant after π_c (called "constant pressure collapse" and observed for fatty acid monolayers at high subphase pH).[43] In the collapse a metastable thermodynamic equilibrium between the monolayer and the freshly collapsed material can be presumed.[44] For EPA monolayer at pH 1.8 the "freshly" collapsed state seems to arise at the above-mentioned first break in the isotherm, i.e., at $\Pi_{freshly}$ = 34 ± 1 mN m^{-1}. A great deal of overcompression is required when a high enough surface pressure is applied in order to force molecules out of the film when the interactions within the film are strong, as occurs with EPA at low pH values due to the phosphonic–phosphonic hydrogen bonding. When this happens, groups of molecules are squeezed out of the surface, provoking a sort of folding process of the layer under compression, which finally breaks off and lies on the remaining monolayer as collapsed fragments being visible in BAM images as thick bright strips, as described in Figure 8d in the Supporting Information. When multilayers are formed during rapid compression experiments, a further increase in surface pressure occurs.[45] Indeed, in the collapse region of the EPA monolayer spread on subphase of pH 1.8 (Figure 5 in the Supporting Information) two pseudoplateaus can be observed 35 and 49 mN·m^{-1} (minimums in the κ^{-1}–Π curve, inset of

DOI: 10.1021/la5050283
Langmuir XXXX, XXX, XXX–XXX

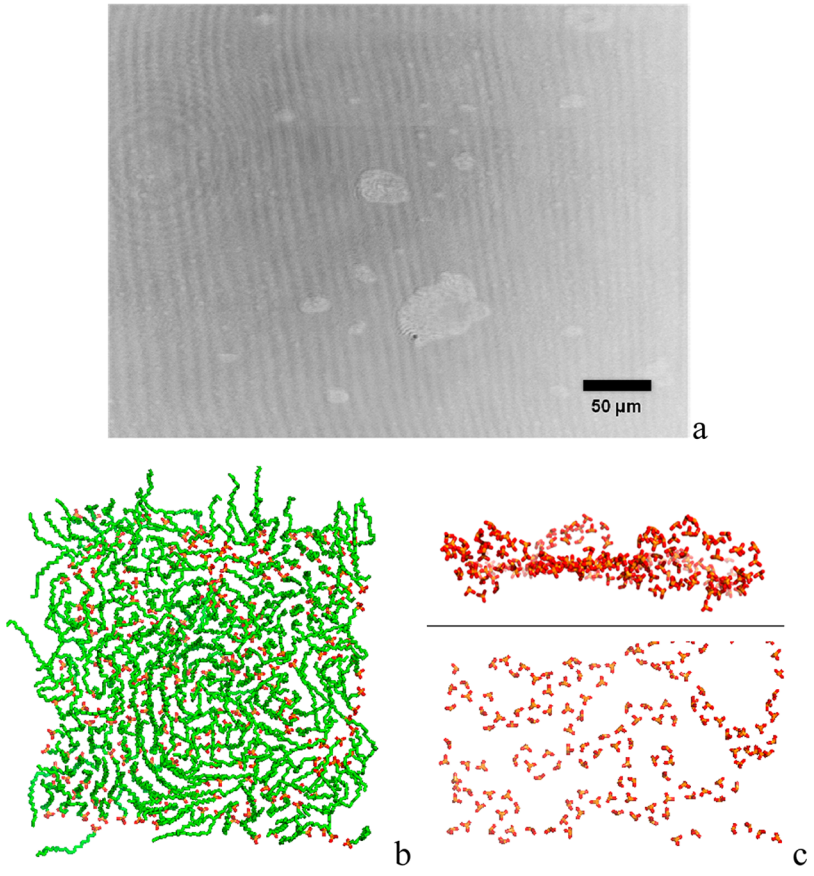

Figure 4. (a) BAM image of the EPA monolayer spread on subphase of pH = 11.81 (Z_{av} = 1.99) showing bubbles of gaseous phase in the LE phase at Π = 1.4 mN m^{-1} and A = 78.2 $Å^2$ $molecule^{-1}$. (b) Upper view of the simulated $C_{20}H_{41}–PO_3^{2-}$ monolayer (hydrocarbon chains in green, P in orange, O in red). (c) Headgroups disposition: lateral view (upper part); upper view (lower part).

Figure 5 in the Supporting Information). These pseudoplateaus could be attributed to the formation of multilayers. Interestingly, the fact that the area corresponding to the fracture collapse (at the end of compression) is approximately one-third of that seen at the first break in the Π–A isotherm (Figure 5 of the Supporting Information) suggests the formation of a trilayer along the collapse region, as was proposed by other authors.[46,47] However, it is worth noting that isotherms reflect an average behavior of the film, and thus the areas and pressures are due to a composition of domains with different layer thickness. Folding occurs for highly rigid monolayers where stretching and shearing modes are expensive in comparison to bending modes. Indeed, the capability of forming extensive hydrogen-bonding networks between phosphonic acid headgroups as well as with water molecules at low pH represents an in-plane resistance to shear allowing an out-of-plane deformation, possibly into multilayers.

When subphase pH is 3.7, the domains group in rows of uniform brightness on compression, to eventually collapse by a fracture mechanism at Π ∼ 53 mN m^{-1} (Figure 8e–g in Supporting Information). The π–A isotherm also shows two pseudoplateaus in the collapse region, suggesting the formation of multilayers (minimums in the κ^{-1}–Π plot at 37.5 and 51.2 mN m^{-1} (inset of Figure 5 in the Supporting Information) and at the respective area values of 21 and 10 $Å^2$ $molecule^{-1}$. The BAM images at the first pseudoplateau show bright patches corresponding to the formation of a layer on the top of the monolayer in a similar way as described by Lipp et al.[48] in the collapse region of mixed films of palmitic acid and 20 wt % of human lung surfactant protein.

Monolayers Behavior at Subphase pH Values of 6.3 and 8.0. The EPA monolayers at 6.3 (Z_{av} ≈ 0.7) and 8.0 (Z_{av} ≈ 1) behave differently to those having lower Z_{av} values (see Figures 1 and 9 in the Supporting Information). This change is in agreement with the change in the behavior of emulsions stabilized with dodecane phosphonic acid evidenced for Z_{av} ≥ 0.47.[18] Both monolayers at the mentioned pH values show a noticeable area expansion due to the increasing degree of surface ionization of the polar headgroups. In this situation the possibility of phosphonic–phosphonic hydrogen bonding is reduced, and there occur changes in the headgroups hydration, in phosphonate–water hydrogen bonding, and in the interaction among the neighboring headgroups (see the MDS results and discussion below), causing an increased film area. Again, a similar conclusion was presented in the interpretation of the behavior of monoalkyl phosphate monolayers when the subphase pH was changed.[6]

It can be observed that at surface pressures below 41 mN m^{-1} both isotherms overlap. They also overlap with the isotherm of pH 9.9 (Figure 1) at a lower surface pressure (24 mN m^{-1}). This behavior suggests that for Z_{av} values between 0.7 and 1.0 (pH 6.3–9.9), there is equilibrium between the total cohesive energy and the electrostatic repulsion. However, at high surface pressures the monolayer surface behavior is quite different as evidenced by BAM images. Figure 10 in the Supporting Information shows the images corresponding to EPA monolayers at pH = 6.3 (images a, b, and c) and pH = 8.0

DOI: 10.1021/la5050283
Langmuir XXXX, XXX, XXX–XXX

(images c, d, and f). In the first case, fingering domains appear at $\Pi \approx 40$ mN m^{-1} and A ≈ 25 Å^2 molecule^{-1}, at the first break in the $\Pi-A$ isotherm (or the first minimum in the corresponding $\kappa^{-1}-\Pi$ curve) (see Figure 3a). These structures do not appear when a concentrated buffer is used and have been observed in the LE−LC coexistence region of different monolayers.[49] Fingering and dendritic domains have been attributed to a restricted movement of the molecules by either the molecular structure of the surfactant[50] or the presence of interfacial hydrogen bonding network of the headgroups.[51] The Coulombic repulsion between charged headgroups, the reduction in hydrogen bonding, and the higher hydration reduce the line tension favoring the fingering of the domains in comparison with the higher line tensions that favor circular domains at lower pH values. Moreover, in a previous work[3] we found that the mean lifetime of hydrogen bonds between phosphonic groups is about 4 orders of magnitude higher than that of water, which means that these hydrogen bonds are much stronger than that between water molecules in bulk. This difference creates the line tension at the border of the islands.

When compression proceeds, the fingering domains come together discontinuously increasing the surface pressure until the collapse by fracture at approximately 53 mN m^{-1} and 7.5 Å^2 molecule^{-1} (inset of Figure 9 in the Supporting Information). This area is about one-third of the corresponding area at the beginning of collapse.

The monolayer spread on the subphase with pH 8.0 ($Z_{av} \approx 1$) behaves differently than the one on the subphase with pH 6.3 ($Z_{av} \approx 0.7$). The first break in the $\Pi-A$ isotherm occurs at a higher area (approximately 31 Å^2 molecule^{-1}) (Figure 9 in the Supporting Information), followed by a continuous increase of the surface pressure with film compression, unlike the previous systems where the increase is discontinuous. Besides, the collapse occurs via a nucleation and growth process. Indeed, BAM images obtained along the collapse region (Figure 10d−f in the Supporting Information) show the initial existence of small collapsed nuclei, which size increases with compression, eventually resulting in the appearance of a uniform distribution of collapsed phase domains across the film.

A visual inspection of the simulation snapshots reveals a greater disorder in the $C_{20}H_{41}-PO_3H^-$ monolayer than in the previous system (see Figures 3b and 11 in the Supporting Information). The clusters of regularly arranged headgroups are no longer observed (Figure 3c).

Monolayers Behavior at Subphase pH Values of 9.9 and 11.8. Figure 12 in the Supporting Information shows the $\Pi-A$ isotherms of EPA monolayers spread on subphases of pH 9.9 ($Z_{av} = 1.6$) and 11.8 ($Z_{av} \approx 2.0$). The corresponding $\kappa^{-1}-\Pi$ curves are also shown in the insets. The high electrostatic repulsion, particularly when the monolayer is fully ionized (pH = 11.8), as well as the stronger hydration of the phosphonate group by ion-dipole interactions between the charged oxygen and water, may explain the existence of larger molecular area values at the beginning of the liquid-expanded phase of these monolayers (>90 Å^2 molecule^{-1}) compared to the results obtained for lower pH subphases (<90 Å^2 molecule^{-1}).

When the subphase has pH 9.9, the first break in the $\Pi-A$ isotherm occurs at 33 Å^2 molecule^{-1} and 41 mN m^{-1}, and as well as in the monolayer with pH 8 subphase, collapse occurs via a nucleation mechanism.

At pH 11.8 the existence of intermolecular hydrogen bridges is negligible, and the monolayer behaves as those of common ionic surfactants. BAM images at the beginning of the compression were homogeneous with occasionally some two-dimensional bubbles of gaseous phase (Figure 4a). When the total area is reduced, the size of these bubbles diminishes, resulting in a homogeneous LE monolayer (Figure 13a,b in the Supporting Information). Immediately after the first break in the $\Pi-A$ isotherm, the whole air−water interface was covered with small crystalline nuclei (Figure 13c in the Supporting Information), which become more visible with the monolayer compression due to the increase of the nucleation density (Figure 13b in the Supporting Information). In contrast to monolayers with lower subphase pH values, a large plateau in the collapse region from 38.5 to 43 mN m^{-1} is observed in the $\Pi-A$ isotherm.

Figure 4b shows an upper view of the simulated $C_{20}H_{41}-PO_3^{2-}$ monolayer, which is much more disordered than in the previous systems and the spiral is no longer present. Because of the lack of hydrogen bonds and the electrostatic repulsion, the monolayer is more dispersed. Figure 4c shows the headgroups tendency to keep distanced between them not only in the *xy* plane but also in the *z* direction. This configuration seems to be the responsible for the large plateau observed in the experimental monolayer at pH = 11.8 ($Z_{av} \approx 2$). Stearic acid monolayers with more than 98% ionization degree show a surface-roughening collapse due to monolayer buckling which grows on a long time scale.[52]

In a fluid collapse, as occurs in softer and more disordered phases (as in this case, see the hydrocarbon chains packed disorderly in Figure 14 in the Supporting Information), material can randomly leave the surface by flow at some critical pressure (in-plane stress) since a fluid has a minimal penalty for shearing.[42]

A literature value of the excluded area is 35 ± 13 Å^2 in *n*-alkanephosphonic acid-soluble monolayers,[2] which is close to the collapse area in all the experimental isotherms.

Comparative Study of EPA Monolayers as a Function of the Ionization State. Figure 5 shows the P−P radial distribution function (rdf) computed by MDS for the $C_{20}H_{41}-PO_3H_2$, $C_{20}H_{41}-PO_3H^-$, and $C_{20}H_{41}-PO_3^{2-}$ monolayers. With regard to the $C_{20}H_{41}-PO_3H_2$ monolayer, there are two predominant positions for the first phosphorus neighbors, as seen in Figure 6 in the Supporting Information and in Figure 2c: when the phosphorus are in a sort of hydrogen-bonded

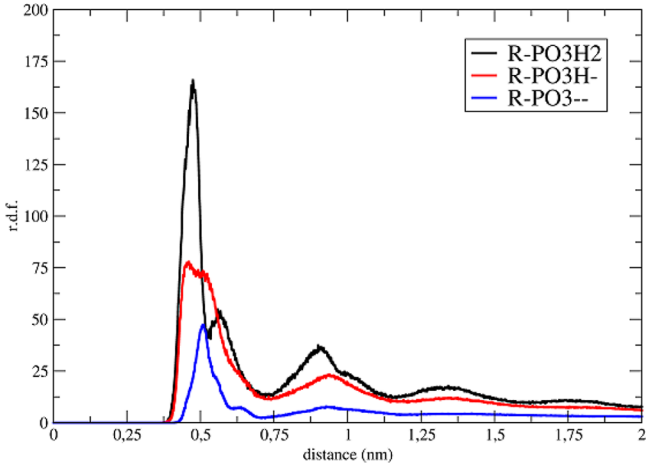

Figure 5. Phosphorus−phosphorus radial distribution function for the $C_{20}H_{41}-PO_3H_2$; the $C_{20}H_{41}-PO_3H^-$ and the $C_{20}H_{41}-PO_3^{2-}$ monolayers at $A = 55$ Å ($Z_{av} = 0$), 68 Å ($Z_{av} = 1$), and 31 Å ($Z_{av} = 2$).

DOI: 10.1021/la5050283
Langmuir XXXX, XXX, XXX−XXX

string, they are at a distance of approximately 4.7 Å, and when they are in parallel strings, the closest distance is ~5.4 Å. These predominant distances correspond to the two first maxima of the phosphorus−phosphorus radial distribution function in Figure 5. In a previous work we have studied both experimentally and by MDS disk-like micelles of *n*-decanephosphonic acid ($C_{10}H_{21}-PO_3H_2$)[3] where the first peak of the P−P rdf is also at 4.7 Å. In the $C_{20}H_{41}-PO_3H^-$ monolayer there are fewer hydrogen bonded groups and there is electrostatic repulsion between the headgroups; thus, the two peaks corresponding to the first coordination layer are of almost the same magnitude and superimposed. This effect is magnified in the $C_{20}H_{41}-PO_3^{2-}$ monolayer, where the first maximum in the P−P rdf is at ~5.3 Å. The electrostatic repulsion and the dwindling hydrogen bonding are also manifested by the start of the rdf curves: 3.8 Å for $Z = 0$ and $Z = 1$ but 4.3 Å for $Z = 2$. The attenuation of the peaks at increasing radial distances from the central particle indicates the decreasing degree of order. This lost of long-range order is evident in the $C_{20}H_{41}-PO_3^{2-}$ monolayer while in the monolayers retaining the ability to form hydrogen bonds the order is maintained for longer distances. The relation between areas below the rdf curves up to 20 Å is 37.47:27.79:7.16 for $Z = 0$:1:2, quantifying the reduction of compactness of the monolayer when the absolute value of Z is increased. This is compatible with the gradual reduction in the attractive interactions between polar headgroups, evidenced in Figure 1 with the expansion of the Π−*A* isotherm when the charge of the phosphonate groups is decreased from 0 to −2.

Figure 13 in the Supporting Information shows the mean number of hydrogen bonds per polar headgroup as a function of time and ionization, considering a geometric criteria for the hydrogen bond identification (cutoff: 30° and 3.5 Å). The number of hydrogen bonds per polar headgroup in the $C_{20}H_{41}-PO_3H_2$ monolayer is about 1, i.e., each molecule is bounded to other two; while in the $C_{20}H_{41}-PO_3H^-$ monolayer is about 0.5, in complete agreement with the reduction of the first peak of the P−P rdf of the corresponding monolayers (Figure 5).

The film area in the close-packed state of the monolayers (area A_i at the first break in the Π−*A* isotherms) increases relatively slow when the polar headgroups are able to form hydrogen bonds but becomes nearly twice that of the uncharged acid when the phosphonic groups are entirely ionized ($Z_{av} \approx 2$), and the electrostatic repulsion between them is noticeable. Figure 16 in the Supporting Information shows A_i vs Z_{av}, where the A_i values were obtained from the first minimum in the compressional modulus molecule^{-1}, concordant with literature values for similar compounds. Indeed, for mono-*n*-octadecylphosphoric acid the limiting area at low degree of surface ionization was 25.5 Å^2. curves. Between pH 1.8 and 6.3 ($Z_{av} = 0-0.7$) the area increases from 22 to 25 Å^2 molecule^{-1},[53] slightly higher than the obtained in this work for pH 1.8, which seems reasonable since the limiting areas were obtained by drawing a tangent in the Π−*A* isotherms from the start of the collapse to zero pressure, while the A_i values were obtained from the $\kappa^{-1}-A$ curve at the first minimum; i.e., both area values are determined at different surface pressures. The value of 25 Å^2 molecule^{-1} obtained by us at pH 6.3 is between that obtained by Gerhsfeld and Pack[26] (24.2 Å^2 molecule^{-1} at pH 5.8) and by He et al.[54] (26 Å^2 molecule^{-1} at pH 5.6), both corresponding to mono-*n*-octadecylphosphoric acid. The increase of pH from 6.4 to 8.0 ($Z_{av} = 0.7-1$) resulted in a shift of the isotherms to significantly greater areas, namely twice that observed in the pH range 1.8−6.3. This is reflected on A_i which rises due to the increasing repulsion among the charged headgroups and the gradual weakening of the hydrogen-bonded network of the polar headgroups, mainly occurring in the Z_{av} region of 0.7−1.0. Above this region a pseudoplateau is observed in the A_i vs Z_{av} curve. At pH values higher than 9.9 there is a large expansion in the isotherm (Figure 1), and thus A_i for $Z_{av} \approx 2$ is twice the value for the uncharged film, indicating that the cohesive energy can no longer counteract the electrostatic repulsion among charged headgroups.

Hydration of the polar headgroups and the first and second methylene groups of the hydrocarbon chains for the three ionization states are interpreted through the rdf of the water oxygen atoms (O) with respect to the phosphorus (P) atom and the first (C_1) and second (C_2) carbon atoms obtained from MDS results (Figure 17 in the Supporting Information). It can be observed that the first hydration layer of the phosphorus atoms does not seem to be much affected by the charge of the polar headgroup: the position of the first peak is shifted from 0.377 nm ($C_{20}H_{41}-PO_3H_2$) to 0.384 nm ($C_{20}H_{41}-PO_3H^-$ and $C_{20}H_{41}-PO_3^{2-}$). The main difference is that the P−O rdf of $C_{20}H_{41}-PO_3^{2-}$ shows two secondary hydration layers extended up to ~0.65 nm. The separation between the polar headgroups allows the formation of several layers of water oriented by the structure of the first coordination shell. The long-range electrical influence of the group with $Z_{av} = 2$ contributes to this structure arrangement. However, as the phosphonate groups in the $C_{20}H_{41}-PO_3H_2$ and $C_{20}H_{41}-PO_3H^-$ monolayers strongly interact via hydrogen bonds, they are too close to each other and have no room for several hydration shells.

The C_1−O rdf has the first maximum at 3.4 Å in the $C_{20}H_{41}-PO_3H_2$ monolayer, and it is shifted to ~3.7 Å in the $C_{20}H_{41}-PO_3H^-$ and $C_{20}H_{41}-PO_3^{2-}$ monolayers. It seems that the C_1 is less hydrated in the $C_{20}H_{41}-PO_3H^-$ monolayer than in the un-ionized one. The ion-dipole interaction between the charged oxygen and water forms a strong ionic hydration layer structure that hinders the formation of the hydrophobic hydration of hydrocarbon groups.

The rough polar layer in the $C_{20}H_{41}-PO_3^{2-}$ monolayer allows a high interrelation between successive hydration layers enhanced by the structuring action of hydrocarbons on water, as evidenced by the several peaks in the C_1−O rdf.

The hydration of the second methylene group in the $C_{20}H_{41}-PO_3H_2$ and $C_{20}H_{41}-PO_3H^-$ monolayers is lower than in the $C_{20}H_{41}-PO_3^{2-}$ monolayer due to the more open structure of the latter. A visual inspection of the two-charged surfactant monolayer allows the detection of hydrocarbon chains bended like hooks with the portion near the headgroups in contact with the subphase (Figure 14 in the Supporting Information), very similar to the chain arrangement observed in soluble surfactants monolayers. These monolayers show "wetter" portions of the chain; for instance, approximately the first 3.5 methylene groups of the tetradecyltrimethylammonium bromide molecules in the monolayer are "wet".[55] The surfactants in insoluble monolayers interact more weakly with the aqueous subphase than soluble homologues do. Then they tend to be less strongly hydrated which reduces the steric repulsion between adjacent headgroups and enables the molecules to pack more tightly into the monolayer.[38] Moreover, the formation of strong hydrogen bonds among the phosphonic groups enhances this tendency. The above findings are consistent with the previous discussion about A_i.

DOI: 10.1021/la5050283
Langmuir XXXX, XXX, XXX−XXX

The distribution of the heights of the molecules, computed as the difference of the z coordinate of the last (C_{20}) and first (C_1) carbon atoms is presented in Figure 18 in the Supporting Information. The length of a liquid eicosane chain is given by[56]

$$l\ (\text{nm}) = 0.13n_C + 0.1704 = 2.77\ \text{nm} \quad (1)$$

Then, on the assumption that the chain is fully extended, the angle formed by the chain with the plane of the interface (τ) can be computed as sin τ = height/l (see Figure 6 inset). This

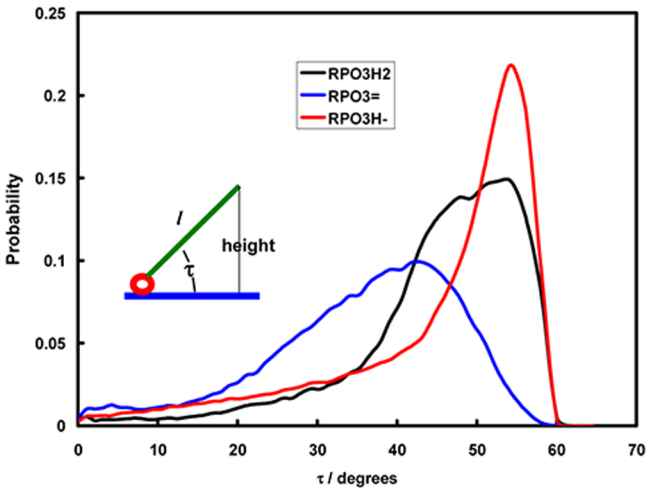

Figure 6. Distribution of angles between the chains and the surface for different values of Z_{av}.

gives for $C_{20}H_{41}-PO_3H_2$ a broad distribution of τ with half-height width between 40.5° and 60.0° and maximum at 54.3° (about 35° from the vertical). The distribution for $C_{20}H_{41}-PO_3H^-$ is narrower with half-height width between 49.3° and 58.0° and maximum at 54.3°. For $C_{20}H_{41}-PO_3^{2-}$ the distribution is broader, with half-height width between 26.8° and 50.9° and a maximum at 43.3° (Figure 6). These values are close to the average tilt found by neutron reflectivity for the chains of hexadecyltrimethylammonium bromide (HTAB) and for dodecyltrimethylammonium bromide at the air/water interface.[57,58] Of course, these tilt angles are only estimations since there is a distribution of tilts of the chains and it is not the same along the chain (Figures 2–4 and Figures 7, 11, and 14 in the Supporting Information), but in light of the experimental results of different systems, our results seem quite reasonable. Lu et al.[57,58] found in HTAB monolayers that half of the hydrocarbon tails closer to the polar headgroup is oriented almost vertical to the surface, while the distal half is more and more tilted. The same authors also found that the reduction of the area per molecule leads to a decrease of the inclination of the chains and vice versa. The bimodal distribution for $C_{20}H_{41}-PO_3H_2$ may be caused by the different orientations of the chains in the spiral as discussed when analyzing Figure 2. Besides, it has been determined that the islands of octadecylphosphonic acid on mica have a height of 1.8 ± 0.2 nm,[35] and it has been interpreted that this implies that, as the length of a fully extend molecule is 2.5 nm, either that the hydrocarbon chain has a 40° tilt angle with respect to the surface or that the chain is significantly disordered.

Other characteristic parameters of the monolayers are the area, A_{coll}, and the surface pressure, Π_{coll}, corresponding to the collapse (either by fracture or by nucleation). They have been plotted as a function of Z_{av} in Figures 19 and 20 of the Supporting Information.

The values are averages from several repeated isotherms. The confidence intervals superimpose, meaning that the differences in the average values have not statistic significance. The weighted average values have been computed with the Student t probability distribution and a 90% confidence level, being A_{coll} = 8.24 ± 0.23 Å^2 molecule^{-1} and Π_{coll} = 49.4 ± 1.2 mN m^{-1}, and are independent of the subphase pH within experimental errors. The related surfactant di-*n*-dodecylphosphoric acid has a collapse pressure of ~50 mN m^{-1}, while the isomers having two chains with 14, 16, and 18 carbon atoms each have a collapse pressure Π_{coll} ~ 60 mN m^{-1}.[54]

On the basis of some characteristics of the isotherms (*vide supra*), it may be considered that the EPA monolayers are composed by mixtures of $C_{20}H_{41}-PO_3H_2$ and $C_{20}H_{41}-PO_3H^-$ for Z_{av} < 1 or by $C_{20}H_{41}-PO_3^{2-}$ and $C_{20}H_{41}-PO_3H^-$ for 1 < Z_{av} < 2. For these mixtures the interactions between the components can be studied considering their miscibility. Intermolecular interactions between components determine whether they behave ideally. If two components are ideally miscible or immiscible, the plot of properties, such as the mean area per molecule, as a function of mixture composition is a straight line.[45] Figure 7 shows the plot of the mean area per

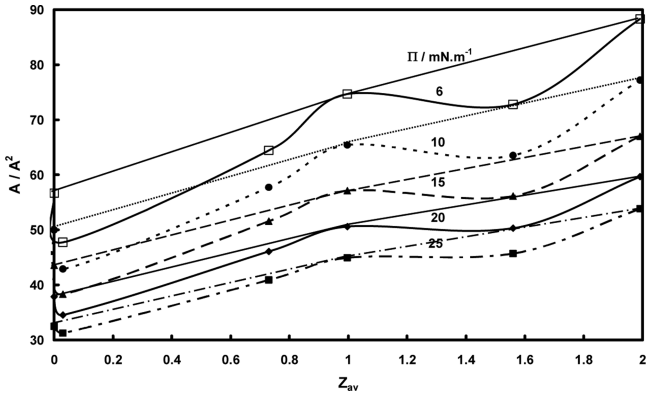

Figure 7. Measured (symbols) and ideal (straight lines) average surface areas per molecule at different surface pressures as a function of the average charge per adsorbed molecule. The curves are eye guides.

molecule as a function of Z_{av} for Π = 6, 10, 15, 20, and 25 mN m^{-1}. Since there is no linearity at the different surface pressures, it is evident that the components are miscible and interact between them. The interaction is attractive because the measured average area is lower than the ideal one, indicating a high packing efficiency. When Π increases, the difference between measured and ideal areas decreases as expected since at higher surface pressures the packing is more compact and the effect of hydrogen bonds is less important.

Figure 21 in the Supporting Information shows the deuterium order parameters (Scd) as a function of the carbon atoms in the chain. As discussed in the Supporting Information, it may bde concluded that that the packing of the $C_{20}H_{41}-PO_3^{2-}$ monolayer is much looser than the other two. Besides, although the packing of the headgroups, and hence the first CH_2 groups, is tighter in the $C_{20}H_{41}-PO_3H_2$ than in the $C_{20}H_{41}-PO_3H^-$, this situation is inverted in the rest of the chain, with the C atom density lower for the $C_{20}H_{41}-PO_3H_2$.

DOI: 10.1021/la5050283
Langmuir XXXX, XXX, XXX–XXX

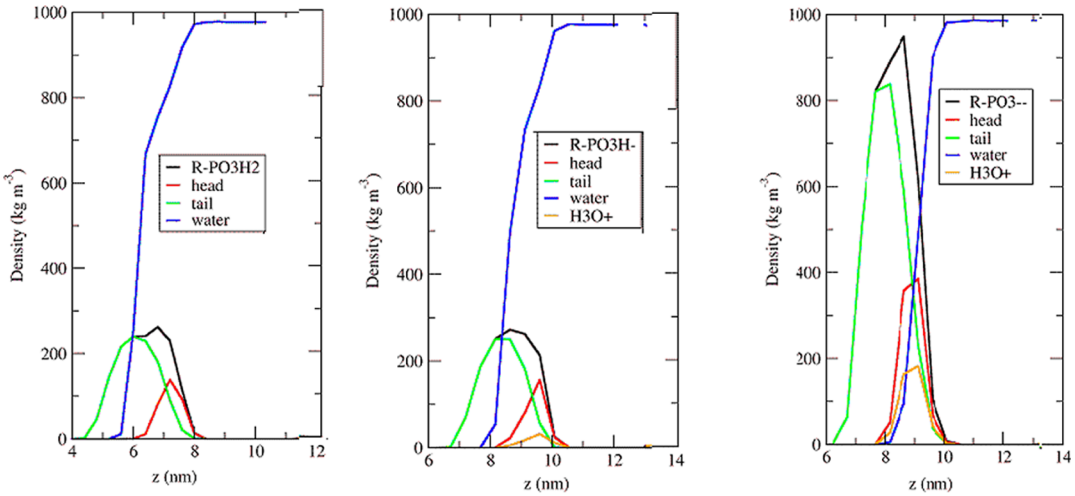

Figure 8. Density profiles of the $R-PO_3H_2$ (left), $R-PO_3H^-$ (center), and $R-PO_3^{2-}$ (right) monolayers.

Figure 8 shows the density profiles of the $C_{20}H_{41}-PO_3H_2$, $C_{20}H_{41}-PO_3H^-$, and $C_{20}H_{41}-PO_3^{2-}$ monolayers obtained with MDS in agreement with the general features of our experimental findings. These distributions resemble the obtained from neutron reflection experiments on surfactant monolayers such as hexadecyltrimethylammonium bromide (HTAB) at the air/water interface.[38] In the $C_{20}H_{41}-PO_3H_2$ and $C_{20}H_{41}-PO_3H^-$ monolayers the polar heads are completely immersed in the subphase, while the tails seem to be partially immersed. However, in the $C_{20}H_{41}-PO_3^{2-}$ monolayer the interface is not sharply defined due to the polar layer roughness. In soluble monolayers such as that of HTAB, about 25% of the tail is inside the aqueous subphase.[55] However, this is an average value whose interpretation is not unique, especially because in soluble monolayers the packing is very loose allowing to a considerable disorder in the monolayer. This behavior is consistent with the fact that the structure breaking effect of phosphonate groups increases when Z_{av} decreases, being the $-PO_3H_2$ group a strong structure breaker of water.[59] When the water structure is broken, the solubility of hydrocarbons increases, in concordance with our observations.

It must be taken into account that the plots of the density distributions are partially determined by the capillary wave roughness and the average overlap between the distributions of water, headgroups, and tails is not necessarily the same as the local overlap.[60] The roughness of a layer at the air/water interface is manifested both in the width of the surfactant distribution and in the range over which the water distribution declines from solution to vapor phase. Then, the distribution profiles of the $C_{20}H_{41}-PO_3^{2-}$ monolayer in Figure 8 is compatible with the low wetting of the chains determined in Figure 17 of the Supporting Information. The surface roughness of the air/water interface in aqueous HTAB at the critical micelle concentration was estimated by Lu et al.[60] as 9.2 Å, which is bigger than the overlap between the tails and the water distributions (Figure 8). The same authors concluded that in HTAB monolayers the local surface roughness can originate a substantial part of the overlapping between the different components distributions at the air/water interface. It must also be taken into account that the charge of the fully ionized phosphonate groups is twice that of the surfactants commonly studied, such as HTAB, and this increased repulsion must also cause an effect on the film properties, such as facilitate the squeezing out of the headgroups; i.e., the tails are out of the average surface of water.

As expected, the distribution of counterions (H_3O^{+}) is almost the same that of the charged polar headgroups. Although in the three cases the surface tension is very similar, the chain density for $Z_{av} = 2$ is much higher since, due to the dispersion in the z direction of the headgroups (Figure 4c), the area of the simulation box in the xy plane is smaller.

CONCLUSIONS

The whole range of ionization states of *n*-eicosanephosphonic monolayers has been studied experimentally, using a Langmuir balance and a Brewster angle microscope, by varying the subphase pH, and by MDS. The monolayers behave as mixtures of the different miscible species ($C_{20}H_{41}-PO_3H_2$, $C_{20}H_{41}-PO_3H^-$, and $C_{20}H_{41}-PO_3^{2-}$) depending on the subphase pH, with nonideal attractive interaction of the molecules. When $Z_{av} \approx 0$ (pH = 1.8), the monolayer is strongly interconnected by phosphonic−phosphonic hydrogen bonds what causes the appearance of rounded and spiraled islands of condensed phase in a gaseous matrix. MDS show that in such islands the molecules are tilted away from the vertical and there clusters of regularly arranged headgroups, in concordance with a L_2 phase. When the pH subphase is between 1.8 and 3.7 ($0.03 < Z_{av} < 1.6$), there is an equilibrium between the total cohesive energy and the electrostatic repulsion, causing the superimposition of the isotherms. Fingering domains have been identified which are a consequence of the lower line tension and are usually attributed to a restricted movement of the molecules, in this case to the hydrogen bonds. However, the clusters of regularly arranged headgroups are no longer observed in the MDS. The compressional moduli suggest a LE behavior of the monolayers in the previous cases, what can be assigned to the interaction of the islands or the fingering domains, i.e., not interpreted on the basis of individual molecules. A further increase in Z_{av} provokes the destruction of the hydrogen-bonded network of polar headgroups. For high ionization states, the monolayer buckles since the molecules are more disordered and distanced, not only in the xy direction but also in the z direction. Therefore, a large plateau is observed in the experimental monolayer at pH = 11.8. The monolayers responses to the compressive stresses in the collapse region are consistent with the structures and domains founds in the different ionization states and their

DOI: 10.1021/la5050283
Langmuir XXXX, XXX, XXX−XXX

consequent in-plane rigidity: there is a transition from a solid-like response at low pH subphases, when the extensive hydrogen-bonding networks impose an in-plane resistance to shear favoring the formation to multilayers, to a fluid-like response at high pH subphases, with material randomly leaving the surface as reported in surface-roughening collapses in softer and more disordered phases. A detailed atomistic scope has been achieved from MDS results. When increasing Z, the dwindling ability to form hydrogen bonds is manifested in an evident lost of long-range order and compactness, as evidenced by radial distribution functions. Thus, the more open structures at higher ionization states allow a better hydration of the phosphonic groups and the first part of the hydrocarbon chains.

■ ASSOCIATED CONTENT

Ⓢ Supporting Information

Figures 1−21. This material is available free of charge via the Internet at http://pubs.acs.org.

■ AUTHOR INFORMATION

Corresponding Author

*E-mail erica.schulz@uns.edu.ar (E.P.S.).

Notes

The authors declare no competing financial interest.

■ ACKNOWLEDGMENTS

E.P.S. and M.A.F. are adjunct researchers of the Argentine National Council of Scientific and Technical Research (CONICET). E.P.S. thanks CONICET for a grant that enabled her to travel to the University of Santiago de Compostela (Spain) to do this research. This research was supported by a grant of the Universidad Nacional del Sur, Argentina, and a grant MICINN-Spain (MAT2011-25501). We are grateful to the Centro de Supercomputación de Galicia (CESGA) for computing time.

■ REFERENCES

(1) Zhou, Y.; Raphael, R. M. Solution pH Alters Mechanical and Electrical Properties of Phosphatidylcholine Membranes: Relation between Interfacial Electrostatics, Intramembrane Potential, and Bending Elasticity. *Biophys. J.* **2007**, *92*, 2451−2462.

(2) Schulz, P. C. Phosphonate Surfactants. *e-Gnosis* **2002**, *I*, 1−15.

(3) Schulz, E. P.; Piñeiro, A.; Rodríguez, J. L.; Minardi, R. M.; Frechero, M.; Schulz, P. C. Intermediate Structures for Higher Level Arrangements: Catching Disk-Like Micelles in Decane Phosphonic Acid Aqueous Solutions. *J. Phys. Chem. B* **2013**, *117*, 6231−6240.

(4) Klose, G.; Petrov, A. G.; Volke, F.; Meyer, H. W.; Förster, G.; Rettig, W. Self-Assembly and Phase Behavior of Short Chain Phosphonic Acid-Water Systems in a Wide Concentration Range. *Mol. Cryst. Liq. Cryst.* **1982**, *88*, 109−126.

(5) Verdinelli, V.; Vuano, B.; Schulz, P. C.; Messina, P. V. Inversion Properties of n-Alkane Phosphonic Acids Stabilized Emulsions: HLB Dependence. *J. Dispersion Sci. Technol.* **2009**, *30*, 1538−1544.

(6) Verdinelli, V.; Messina, P. V.; Schulz, E. N.; Salinas, D.; Vuano, B.; Schulz, P. C. The Effect of the Hydrocarbon−Water Interface Structure on the Behavior of an Emulsion Stabilized with Dodecanephosphonic Acid. *Colloids Surf., A* **2010**, *367*, 1−6.

(7) Blanco, E.; Piñeiro, A.; Miller, R.; Ruso, J. M.; Prieto, G.; Sarmiento, F. Langmuir Monolayers of a Hydrogenated/Fluorinated Catanionic Surfactant: From the Macroscopic to the Nanoscopic Size Scale. *Langmuir* **2009**, *25* (14), 8075−8082.

(8) Yuan, S.; Ma, L.; Zhang, X.; Zheng, L. Molecular Dynamics Studies on Monolayer of Cetyltrimethylammonium Bromide Surfactant Formed at the Air/Water Interface. *Colloids Surf., A* **2006**, *289*, 1−9.

(9) Hassan, N.; Russo, J. M.; Piñeiro, A. Hydrogenated/Fluorinated Catanionic Surfactants as Potential Templated for Nanostructure Design. *Langmiur* **2011**, *27*, 9719−9728.

(10) Piñeiro, A.; Prieto, G.; Ruso, J. M.; Verdes, P. V.; Sarmiento, F. Surface Films of Short Fluorocarbon- Hydrocarbon Diblocks Studied by Molecular Dynamics Simulations: Spontaneous Formation of Elongated Hemmicelles. *J. Colloids Interface Sci.* **2009**, *329*, 351−356.

(11) Woodhead, J: L.; Hall, C. K. Simulation of Micelle Formation in the Presence of Solutes. *Langmuir* **2010**, *26* (19), 15135−15141.

(12) Duncan, S. L.; Larson, R. G. Comparing Experimental and Simulated Pressure-Area Isotherms for DPPC. *Biophys. J.* **2008**, *94*, 2965−2986.

(13) Dzieciol, A. J.; Mann, S. Designs for Life: Protocell Models in the Laboratory. *Chem. Soc. Rev.* **2012**, *41*, 79−85.

(14) Adden, N.; Gamble, L. J.; Castner, D. G.; Hoffmann, A.; Gross, A.; Menzel, H. Phosphonic Acid Monolayers for Binding Bioactive Molecules to Titanium Surfaces. *Langmuir* **2006**, *22*, 8197−8204.

(15) Kanta, A.; Sedev, R.; Ralston, J. The Formation and Stability of Self-Assembled Monolayers of Octadecylphosphonic Acids on Titania. *Colloids Surf., A* **2006**, *291*, 51−58.

(16) Balachandian, S. R.; Simkovich, C.; Arlan, F. F. The Influence of Point Defects on the Floatability of Cassiterite, III. the Role of Collector Type. *Int. J. Miner. Process.* **1987**, *21* (3-4), 185−203.

(17) Mikroyannidis, J. A. Hydroxy and/or Carboxy Substituted Phosphonic and Bisphosphonic Acids Usable As Corrosion and Scale Inhibitors. *Phosphorus Sulphur* **1987**, *32*, 113−118.

(18) Roy, S.; Ataol, T. M.; Muller-Plathe, B. Molecular Dynamics Simulation of Heptyl Phosphonic Acid: A Potential Component for Fuel Cell Polymer Membrane. *J. Phys. Chem. B* **2008**, *112*, 7403−7409.

(19) Cooper, G. W.; Lnwo, W. M. O.; Cronin, J. R. Alkyl Phosphonic Acids and Sulfonic Acids in the Murchison Meteorite. *Geochim. Cosmochim. Acta* **1992**, *56*, 4109−4115.

(20) de Graaf, R. M; Visscher, J.; Schwartz, A. W. A Plausibly Prebiotic Synthesis of Phosphonic Acids. *Nature* **1995**, *378*, 474−477.

(21) Gorrell, I. B.; Wang, L.; Marks, A. J.; Bryant, D. E.; Bouillot, F.; Goddard, A.; Heard, D. E.; Kee, Y. P. On the Origin of the Murchison Meteorite Phosphonates. Implications for Pre-Biotic Chemistry. *Chem. Commun.* **2006**, 1643−1645.

(22) Palm, K.; Luthman, K.; Ros, J.; Gråsjo, J.; Artursson, P. Effect of Molecular Charge on Intestinal Epithelial Drug Transport: pH-Dependent Transport of Cationic Drugs. *J. Pharmacol. Exp. Ther.* **1999**, *291*, 435−443.

(23) Ricciardi, R.; Huskens, J.; Verboom, W. Heterogeneous Acid Catalysis Using a Perfluorosulfonic Acid Monolayer-Functionalized Microreactor. *J. Flow Chem.* **2013**, *3* (4), 127−131.

(24) Vogel, N.; Weiss, C. K.; Landfester, K. From Soft to Hard: the Generation of Functional and Complex Colloidal Monolayers for Nanolithography. *Soft Matter* **2012**, *8*, 4044−4061.

(25) Bernardi, M.; Palummo, M.; Grossman, J. C. Extraordinary Sunlight Absorption and One Nanometer Thick Photovoltaics Using Two-Dimensional Monolayer. *Mater. Nano Lett.* **2013**, *13*, 3664−3670.

(26) Gershfeld, N. L.; Pak, C. Y. C. The Surface Chemistry of Monooctadecyl Phosphate at the Air/Water Interface. A Study of Molecular Aggregation Monolayers. *J. Colloid Interface Sci.* **1967**, *23*, 215−220.

(27) Kosolapoff, G. M. Isomerization of Alkylphosphites 111, "The Synthesis of n-Alkylphosphonic Acids". *J. Am. Chem. Soc.* **1945**, *67*, 1180−1182.

(28) Teorell, H.; Stenhagen, E. Universal Buffer over the pH range 2.0 to 12.0. *Biochem Z.* **1939**, *294*, 417−419.

(29) Miñones, J. *Monolayers and multilayers of Langmuir Blodgett*; Instituto de España, Real Academia de Farmacia: Madrid, 1995; pp 76−7.

(30) Berendsen, H. J. C.; Van de Spoel, D.; van Drunen, R. GROMACS: A Message-Passing Parallel Molecular Dynamics Implementation. *Comput. Phys. Commun.* **1995**, *91*, 43−56. Lindahl, E.; Hess, B.; van der Spoel, D. GROMACS 3.0: a Package for

DOI: 10.1021/la5050283
Langmuir XXXX, XXX, XXX−XXX

Molecular Simulation and Trajectory Análisis. *J. Mol. Model.* **2001**, *7*, 306−317.
(31) Oostenbrink, C.; Villa, A.; Mark, A. E.; van Gunsteren, W. F. A Biomolecular Force Field Based on the Free Enthalpy of Hydration and Solvation: The GROMOS Force-Field Parameter Sets 53A5 and 53A6. *J. Comput. Chem.* **2004**, *25*, 1656−1676.
(32) Berendsen, H. J. C.; Postma, J. P. M.; van Gunsteren, W. F.; Hermans, J. Interaction models for water in relation to protein hydration. In *Intermolecular Forces*; Pullman, B., Ed.; D. Reidel: Dordrecht, 1981; pp 331−342.
(33) Miyamoto, S.; Kollman, P. A. Settle: An Analytical Version of the SHAKE and RATTLE Algorithm for Rigid Water Models. *J. Comput. Chem.* **1992**, *13*, 952−962.
(34) Hess, B.; Bekker, H.; Berendsen, H. J. C.; Fraaije, J. G. E. M. LINCS: A Linear Constraint Solver for Molecular Simulations. *J. Comput. Chem.* **1997**, *18*, 1463−1472.
(35) Rosoff, M. *Nano-Surface Chemistry*; Marcel Dekker Inc.: New York, 2002; Chapter 3.
(36) Woodward, J. T.; Ulman, A.; Schwartz, D. H. Self-Assembled Monolayer Growth of Octadecylphosphonic Acid on Mica. *Langmuir* **1996**, *12*, 3626−3629.
(37) Doudevski, I.; Hayes, W. A.; Schwartz, D. K. Submonolayer Island Nucleation and Growth Kinetics during Self-Assembled Monolayer Formation. *Phys. Rev. Lett.* **1998**, *81* (22), 4927−4930.
(38) Thomas, R. K.; Penfold, J. Neutron and X-ray Reflectometry of Interfacial Systems in Colloid and Polymer Chemistry. *Curr. Opin. Colloid Interface Sci.* **1996**, *1*, 23−33.
(39) Cartmell, E.; Fowles, G. W. A. *Valence and Molecular Structure*; Reverté: Barcelona, 1964; p 148.
(40) Sinnamon, B. F.; Dluhy, R. A.; Barnes, G. T. Reflection-absorption FT-IR Spectroscopy of Pentadecanoic Acid at the Air/Water Interface. *Colloids Surf., A* **1999**, *146*, 49−61.
(41) Gabrielli, G.; Baglioni, P.; Ferroni, E. On the Mechanism of Collapse of Monolayers of Macromolecular Substances: Poly(L,D and DL) alanine. *J. Colloid Interface Sci.* **1981**, *81*, 139−149.
(42) Krishan, K.; Gavrilov, K.; Pocivavsek, L.; Frey, S. L.; Ruchala, P.; Waring, A.; de Frans, J.; Walther, J.; Dennin, M.; Witten, T. A.; Lee, K. Y. C. Lateral Stress Relaxation and Collapse in Lipid Monolayers. *Soft Matter* **2008**, *4*, 2019−2029.
(43) Kundu, S.; Langevin, D. Fatty Acid Monolayer Dissociation and Collapse: Effect of pH and Cations. *Colloids Surf., A* **2008**, *325*, 81−85.
(44) Tomoaia-Cotisel, M.; Zsakó, J.; Mocanu, A.; Lupea, M.; Chifu, E. The Ionization Characteristics of Some Fatty Acids at the Air/Water Interface. *J. Colloid Interface Sci.* **1981**, *117*, 464−476.
(45) Gaines, G. L. *Insoluble Monolayers at Liquid/Gas Interfaces*; Wiley-Interscience: New York, 1966; Chapter 4, p 150.
(46) Ries, H. E. Stable Ridges in a Collapsing Monolayer. *Nature* **1979**, *281*, 287−289.
(47) Ries, Jr., H. E.; Kimball, W. A. Gas/Liquid and Liquid/Liquid Interface. *Proceedings of the 2nd International Congress on Surface Activity*; Butterworths: London, 1957, Vol. *1*, p 75.
(48) Lipp, M. M.; Lee, K. Y. C.; Zasadzinski, J. A.; Waring, A. J. Protein and Lipid Interactions in Lung Surfactant Monolayers. *Prog. Colloid Polym. Sci.* **1997**, *103*, 268−279.
(49) Hönig, D.; Möbius, D. Direct Visualization of Monolayers at the Air-Water Interface by Brewster Angle Microscopy. *J. Phys. Chem.* **1991**, *95*, 4590−4592.
(50) Hossain, Md. M.; Iimura, K.-I.; Kato, T. Temperature and Compression Rate Independent Domain Shape in Langmuir Monolayers of Di-n-Dodecyl Hydrogen Phosphate at the Air-Water Interface. *J. Colloid Interface Sci.* **2008**, *319*, 295−301.
(51) Hossain, Md. M.; Iimura, K.-I.; Yoshida, M.; Kato, T. Temperature Dependent Dendritic Domain Shapes in Langmuir Monolayers of Tetradecanoyl N-Ethanolamide at the Air-Water. *J. Colloid Interface Sci.* **2011**, *353* (2), 220−224.
(52) Hatta, E.; Nagao, J. Topological Manifestations of Surface-Roughening Collapse in Langmuir Monolayer. *Phys. Rev.* **2003**, *E 67*, 041604.
(53) Parreira, H. C. The Surface Chemistry of Alkyl Phosphoric Acids. *J. Colloid Interface Sci.* **1965**, *20*, 742−754.
(54) He, W.; Jiang, C.; Liu, F.; Tai, Z.; Liang, Y.; Guo, Z.; Zhu, L. Monolayer Formation of Alkyl Chain-Containing Phosphoric Acid Amphiphiles at the Air/Water (pH 5.6) Interface: Influence of Temperature and Cations. *J. Colloid Interface Sci.* **2002**, *246*, 335−342.
(55) Simister, E. A.; Lee, E. M.; Thomas, R. K.; Penfold, J. Structure of a Tetradecyltrimethylammonium Bromide Layer at the Air/Water Interface Determined by Neutron Reflection. *J. Phys. Chem.* **1992**, *96*, 1373−1382.
(56) Schulz, P. C. Steric Fitting of the Rodlike Micelle Size. *J. Colloid Interface Sci.* **1992**, *152*, 333−337.
(57) Lu, J. R.; Li, Z. X.; Smallwood, J.; Thomas, R. K.; Penfold, J. Detailed Structure of the Hydrocarbon Chain on a Surfactant Monolayer at the Air/Water Interface: Neutron Reflection from Hexadecyltrimethylammonium Bromide. *J. Phys. Chem.* **1995**, *99*, 8233−8243.
(58) Lu, J. R.; Li, Z. X.; Thomas, R. K.; Penfold, J. Structure of Hydrocarbon Chains in Surfactant Monolayers at the Air/Water Interface: Neutron Reflection from Dodecyl Trimethylammonium Bromide. *J. Chem. Soc., Faraday Trans.* **1996**, *92* (3), 403−408.
(59) Marcus, Y. Effect of Ions on the Structure of Water: Structure Making and Breaking. *Chem. Rev.* **2009**, *109*, 1346−1370.
(60) Lu, J. R.; Thomas, R. K.; Penfold, J. Surfactant Layers at the Air/Water Interface: Structure and Composition. *Adv. Colloid Interface Sci.* **2000**, *84*, 143−304.

DOI: 10.1021/la5050283
Langmuir XXXX, XXX, XXX−XXX